# Radar Stereomapping Techniques and Application to SIR-B Images of Mt. Shasta

FRANZ W. LEBERL, SENIOR MEMBER, IEEE, GITTA DOMIK, JOHANNES RAGGAM, AND MICHAEL KOBRICK

*Abstract*—**One of the goals of the SIR-B experiment was the definition of optimum radar incidence and intersection angles for radargrammetric stereoscopy by comparing the results from three separate data reduction methods. To this end three overlapping images of the prime radargrammetric site (Mt. Shasta in northern California) were obtained, fewer than anticipated. This paper describes the mathematical basis for radar stereomapping, along with preliminary results from one of the methods (using a so-called "analytical" stereoplotter) for the Mt. Shasta site. Height coordinate errors range from 60 to 170 m depending on the density (number per ground area) of ground control points used.**

## I. INTRODUCTION

THE POSSIBILITY of using overlapping radar images for topographic mapping has intrigued researchers for many years, with the first theoretical contribution appearing as early as 1948 [1]. A considerable body of literature has since developed on the subject; however, most work was limited by the unavailability of a range of actual radar image data.

The ability of SIR-B to image targets at different incidence angles on successive days of a one-week mission make it ideal for a radar stereomapping experiment. Therefore, an effort was mounted to collect sets of images of geologic sites which were previously well-mapped so that a systematic stereo experiment could be performed. The objective is to determine the optimum incidence angle combination for both visual interpretation of a geologic site and for topographic mapping.

The overall plan for stereomapping analysis involves independent reduction of the data by three techniques: use of a conventional stereoplotter that has been modified to incorporate radar geometry, a state-of-the-art analytical (or hybrid) analog/digital stereoplotter that incorporates the stereogeometry through software, and computer image-processing techniques for automatic cross correlation of the images. Results of these three coordinated approaches will be compared in an attempt to determine the extent to which the results are technique-dependent and, therefore, the true fundamental accuracy achievable with radar stereo data. This work is still in progress.

This paper presents details of the stereo reduction technique using the hybrid stereoplotter, and some results for the primary test site around Mt. Shasta in northern California. Due to mission anomalies described elsewhere, data for Mt. Shasta fell short of the plan and amounted to only three overlapping images (Fig. 1), one of which suffers from a rather low signal-to-noise ratio. Despite this, the Mt. Shasta data are useful because of the available topographic ground truth (1:62 500 scale contour maps and USGS digital data derived from 1:250 000 scale maps), as well as geologic interest in the site. Mt. Shasta is a volcano of the Cascade chain, which recent results indicate may have undergone a Mt. St. Helens-type explosion of vastly greater magnitude about 350 000 years ago, with the resulting debris flow creating the Shasta valley to the north [2].

Thirty-two ground points were identified in the three images (Fig. 2) and located on the maps. This permitted reduction of three stereomodels and the establishment of an order of magnitude for the achievable point-positioning accuracy, although the data range was insufficient to determine optimum incidence angle combinations.

A more complete data set was obtained for a much less well-mapped area in Argentina, where a total of four images suitable for stereomapping research overlap one another. Analysis of these data is the subject of separate papers in this issue, one of which [7] presents a more complete discussion of the numerical results from both Argentina and Mt. Shasta and an analysis of their accuracy.

## II. STEREOMAPPING METHOD

### A. General Observations

Stereomapping from radar film images on a photogrammetric analytical stereoplotter was demonstrated for the first time by Norvelle [3], and Autometric [4] developed such capability on an APPS-IV and on an AS-11 analytical plotter. Independently, the authors were involved in creating a stereoradar mapping system on a Kern DSR-1/11 instrument. The overall procedure has been described in general terms by Raggam and Leberl [5], and in detail

Manuscript received November 18, 1985; revised February 7, 1986. This work has been supported under a contract between Vexcel Corporation and the Jet Propulsion Laboratory. The participation of M. Kobrick represents one phase of work performed by JPL under Contract NAS 7-100.

E. Leberl and G. Domik are with Vexcel Corporation, Boulder, CO 80301.

J. Raggam is with the Graz Research Center, Graz, A-8010, Austria.

M. Kobrick is with the Jet Propulsion Laboratory, Pasadena, CA 91109.

IEEE Log Number 8608574.

0196-2892/86/0700-0473$01.00 © 1986 IEEE


(a)


(b)

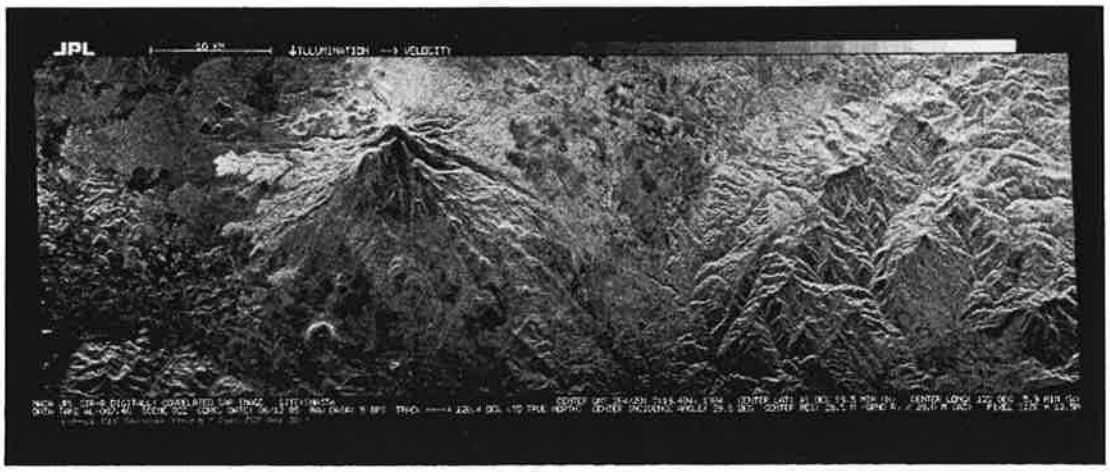


(c)

Fig. 1. SIR-B images of Mt. Shasta, at look angles of 57°, 51°, and 28° off nadir, from an orbit altitude of approximately 230 km, at a wavelength of 25 cm.

in the German language by Raggam [6]. The following is, therefore, a review of the mathematical formulation that has thus far been unavailable in this form.

The overall procedure steps through a stereomodel setup and subsequent real-time data acquisition. The stereomodel setup consists of three steps: a so-called "inner orientation"; a separate "resection-in-space" for each image of the stereopair; and a least squares adjustment of both images simultaneously, using ground control points and additional orientation points. Once this is completed the operator can begin to collect, in real time, ground coordinates of arbitrary points of the stereomodel.

### B. Inner Orientation

Each image is placed on a so-called "plate-carrier" of the analytical plotter. Plate coordinates $\bar{x}$, $\bar{y}$ of an image

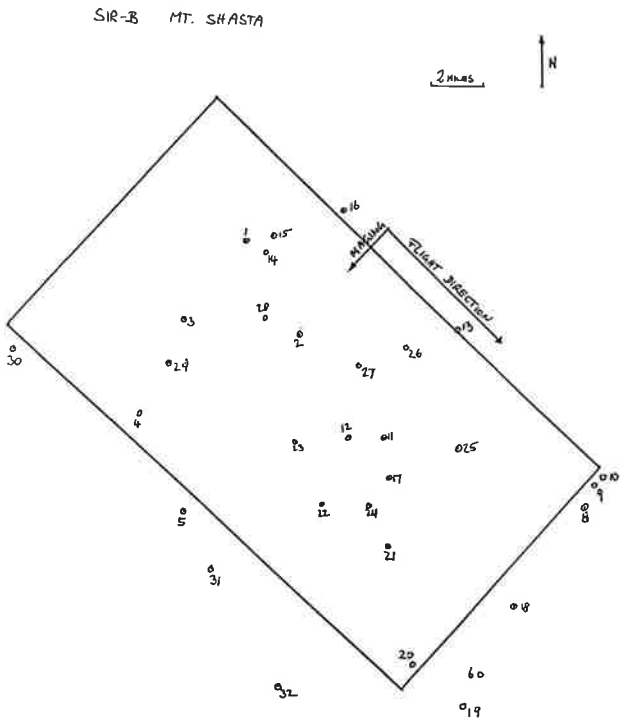


Fig. 2. Distribution of ground control points in the area around Mt. Shasta.

point need to be converted to image coordinates $x$, $y$ by a linear transformation

$$x = b_{11} * x + b_{12} * y + b_{13}$$
$$y = b_{21} * x + b_{22} * y + b_{23}. \quad (1)$$

The transformation parameters $b_{ij}$ are computed from points on a time or range reference line, if such reference is available. In the event of SIR-B data one uses the near-range image edge as a range reference.

The range and time coordinates $r$, $t$ are computed from $x$, $y$ with the help of scale factors $m_x$ and $m_y$ and coordinate shifts $r_0$ and $t_0$

$$r = y * m_y + r_0 \quad (2a)$$
$$t = x * m_x + t_0. \quad (2b)$$

In the event that $m_x$, $m_y$, $r_0$, and $t_0$ are unknown, they will be approximated at this time and determined in subsequent steps.

### C. Projecting Ground Control Points into Images

The next step is the computation of image coordinates $x_p$ and $y_p$ of known ground control points. This is based on previously known or approximated sensor positions and values for the velocity vector of the antenna. The equations are as follows, computing two values $\tau_i$, $\tau_{i+1}$:

$$\sin \tau_i' = \dot{s}' * (\boldsymbol{p} - \boldsymbol{s}_i')/|\dot{\boldsymbol{s}}_i'| * |\boldsymbol{p} - \boldsymbol{s}_i'|$$
$$\sin \tau_{i+1}' = \dot{\boldsymbol{s}}_{i+1}' * (\boldsymbol{p} - \boldsymbol{s}_{i+1}')/|\dot{\boldsymbol{s}}_{i+1}'| \, |\boldsymbol{p} - \boldsymbol{s}_{i+1}'| \quad (3)$$

where $\boldsymbol{p}$ is the position vector of a ground control point, $\boldsymbol{s}_i$ of the satellite at a certain time $t_i$, $\dot{\boldsymbol{s}}_i$ is the velocity vector, and $\tau$ is a squint angle. The prime ($'$) denotes one image; the other is denoted by ($''$). The actual computation is iterative, going through times $t_1, t_2, \cdots, t_n$. The nominal squint angle of the radar device $\tau$ is known. The software algorithm is as follows:

Repeat

$$t_l := t_1 + (t_2 - t_1) * (\sin \tau - \sin \tau_1)/(\sin \tau_2 - \sin \tau_1)$$
$$\boldsymbol{s}_l := \boldsymbol{s}_l(t_l)$$
$$\dot{\boldsymbol{s}}_l := \dot{\boldsymbol{s}}_l(t_l)$$
$$\sin \tau_l := \dot{\boldsymbol{s}}_l * (\boldsymbol{p} - \boldsymbol{s}_l)/|\dot{\boldsymbol{s}}_l| * |\boldsymbol{p} - \boldsymbol{s}_l|$$

If

$$\sin \tau_l > \sin \tau \text{ then } t_1 = t_l$$
$$\sin \tau_1 := \sin \tau_l$$

If

$$\sin \tau_l < \sin \tau \text{ then } t_2 = t_l$$
$$\sin \tau_2 := \sin \tau_l.$$

Until

$$|\sin \tau_l - \sin \tau| < \Delta\tau$$
$$r_s := |\boldsymbol{p} - \boldsymbol{s}_l|$$
$$x := (t_l - t_0)/m_x$$
$$y := (r_s - r_0)/m_y.$$

The value $\Delta\tau$ determines when the iteration is to be terminated. In this manner, every ground point $p$ obtains a computed pair of image coordinates $x'$, $y'$, $x''$, $y''$ in the left and right radar images.

### D. Performing the "Resection-in-Space"

The computed image coordinates $x'$, $y'$ differ from the actually observed ones. This is the basis for a least squares adjustment to minimize the differences and to improve the assumed approximations of orbit positions. The least squares adjustment is based on the following condition equations:

Orbit related

$$a_x + b_x * t + c_x * t^2 + \cdots - s_x = 0.$$
$$a_y + b_y * t + c_y * t^2 + \cdots - s_y = 0.$$
$$a_z + b_z * t + c_z * t^2 + \cdots - s_z = 0. \quad (4)$$

where

$$(s_x, s_y, s_z) = \boldsymbol{s}(t).$$

Range-related

$$r - |\boldsymbol{p} - \boldsymbol{s}| = 0. \quad (5)$$

Squint angle or Doppler-cone related

$$\dot{s} * (p - s) - \sin \tau \, |\dot{s}| \, |p - s| = 0. \quad (6)$$

Each observed orbit station provides three equations (4), each ground point leads to (5) and (6), which in turn contain (4). Computations are repeated with the left- and right-image separately.

A resection-in-space represents a nonlinear equation system and is computed by linearizing the above equations, substituting (2) for $r$ and $t$. In order to avoid numerical instability, all entities are considered to be observed, but are associated with variable weights in the computation to differentiate between poorly known approximations and well-known imaging parameters.

### *E. Stereomeasurements and Stereomodel Setup*

Upon completion of the resection-in-space the operator now moves in a nearly parallax-free stereomodel. However, the process has not yet enforced that conjugate points in the two images indeed have no $y$-parallax and that the corresponding projection rays intersect in object space.

Therefore, additional conjugate (or homologue) image points are observed, and also the ground control points are remeasured stereoscopically. This leads to an equation system with a set of equations (4) and (5) in each image. Each observation of an image coordinate leads to equations of type (4) and (5), two each in the two images.

In order to ensure a parallax-free stereomodel one may measure ten or more conjugate orientation points. Upon completion of the least squares adjustment one has a stereomodel ready for data collection.

### *F. Real-Time Data Collection*

The parameters for the orbit and imaging configuration are available for real-time computation of the image coordinates $x$ and $y$ as the observer moves in the object coordinate system. The analytical plotter operates with a separate processor where the following computation takes place as the operator moves to position $p$, whereby the system just used values with the index $F$ at the previous position

$$\sin \tau_F = \dot{s} * (p - s_F)/|\dot{s}_F| * |p - s_F|$$

If $\sin \tau_F < \sin \tau$

$$\sin \tau := \dot{s}_1 * (p - s_1)/|\dot{s}_1| * |p - s_1|$$

$$t_l := t_1$$

If $\sin \tau_F > \sin \tau$

$$\sin \tau_l := \dot{s}_2 * (p - s_2)/|\dot{s}_2| * |p - s_2|$$

$$t_l := t_2$$

$$t_F := t_F + (t_l - t_F) * (\sin \tau - \sin \tau_F)/(\sin \tau_l - \sin \tau_F)$$

$$s_F := s_F(t_F)$$

$$\dot{s}_F := \dot{s}_F(t_F)$$

$$r := |p - s_F|$$

$$x := (t_F - t_0)/m_x$$

TABLE I
ROOT MEAN SQUARE ERRORS OF GROUND COORDINATES, IN METERS, OBTAINED FROM THE STEREO MODELS FORMED BY THE IMAGES OF FIG. 1
(Input are 4 orbit positions for each image as communicated by the SIRB mission.)

| Control Points | Intersection Angle (°) | Coordinate Errors North | East | Height | Point Error |
|---|---|---|---|---|---|
| | | (in meters) | | | |
| 2 | 6 | 117 | 124 | 155 | 133 |
| 2 | 23 | 44 | 100 | 178 | 120 |
| 2 | 28 | 127 | 134 | 124 | 128 |
| 4 | 6 | 117 | 99 | 113 | 109 |
| 4 | 23 | 45 | 81 | 67 | 66 |
| 4 | 28 | 104 | 121 | 96 | 107 |
| 13 | 6 | 106 | 106 | 125 | 112 |
| 16 | 23 | 44 | 75 | 53 | 58 |
| 17 | 28 | 91 | 100 | 73 | 88 |

TABLE II
PREDICTED STEREORADAR COORDINATE ERRORS
THE PREDICTED ACCURACY IS BETTER THAN THAT ACTUALLY ACHIEVED
(The companion paper on the Argentina data [7] presents some considerations that could explain the discrepancy.)

| Look Angle (°) | Look Angle (°) | Intersection Angle (°) | Error of Height (m) | Error of Position (m) |
|---|---|---|---|---|
| 51 | 57 | 6 | 77 | 56 |
| 28 | 51 | 23 | 16 | 19 |
| 28 | 57 | 28 | 14 | 15 |

$$y := (r - r_0)/m_y$$

$$\bar{x} := b_{11} * x + b_{12} * y + b_{13}$$

$$\bar{y} := b_{21} * x + b_{22} * y + b_{23}.$$

The pair of $xy$ coordinates are in the image system, $\overline{xy}$ are in the plate carrier system. The computation updates the sensor time $t_F$ as one moves through the object space, and this in turn updates the sensor position and other parameters. Collection of object data is provided to include individual points, polygons, contour lines, and DEM grid measurement.

## III. MT. SHASTA MAPPING RESULTS

### *A. Accuracies*

Table I presents the root mean square errors of ground points obtained in the three stereo cases; Table II compares it to predicted values obtained by applying the propagation of image resolution limits into the object coordinates (compare [7, equation (2)] ). It is immediately evident that the largest intersection angle does not produce the best accuracies since the quality of the relevant image at 57° look angle off-nadir is poorer than of other images.

### *B. Digital Elevation Data*

In addition to the accuracy study also a digital elevation model was generated from the stereoradar models (Fig. 3), from the map (Fig. 4), and a difference model is plot-

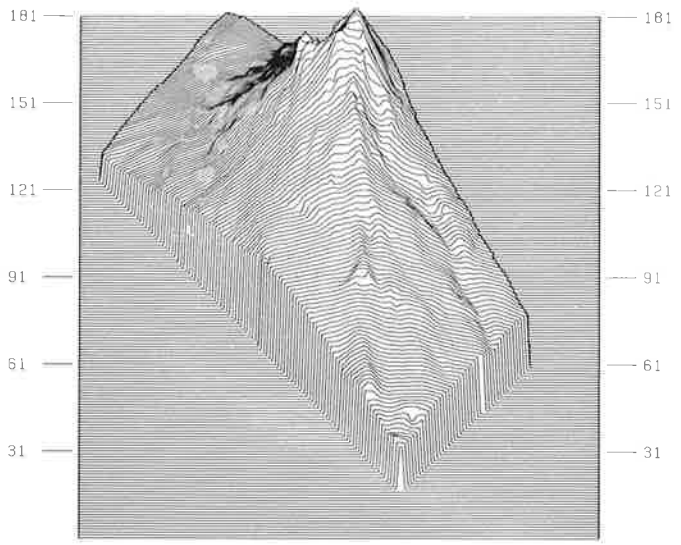


Fig. 3. Digital elevation model created from the SIR-B radar stereopair of 51° and 28° look angles off-nadir, at a grid interval of 150 m.

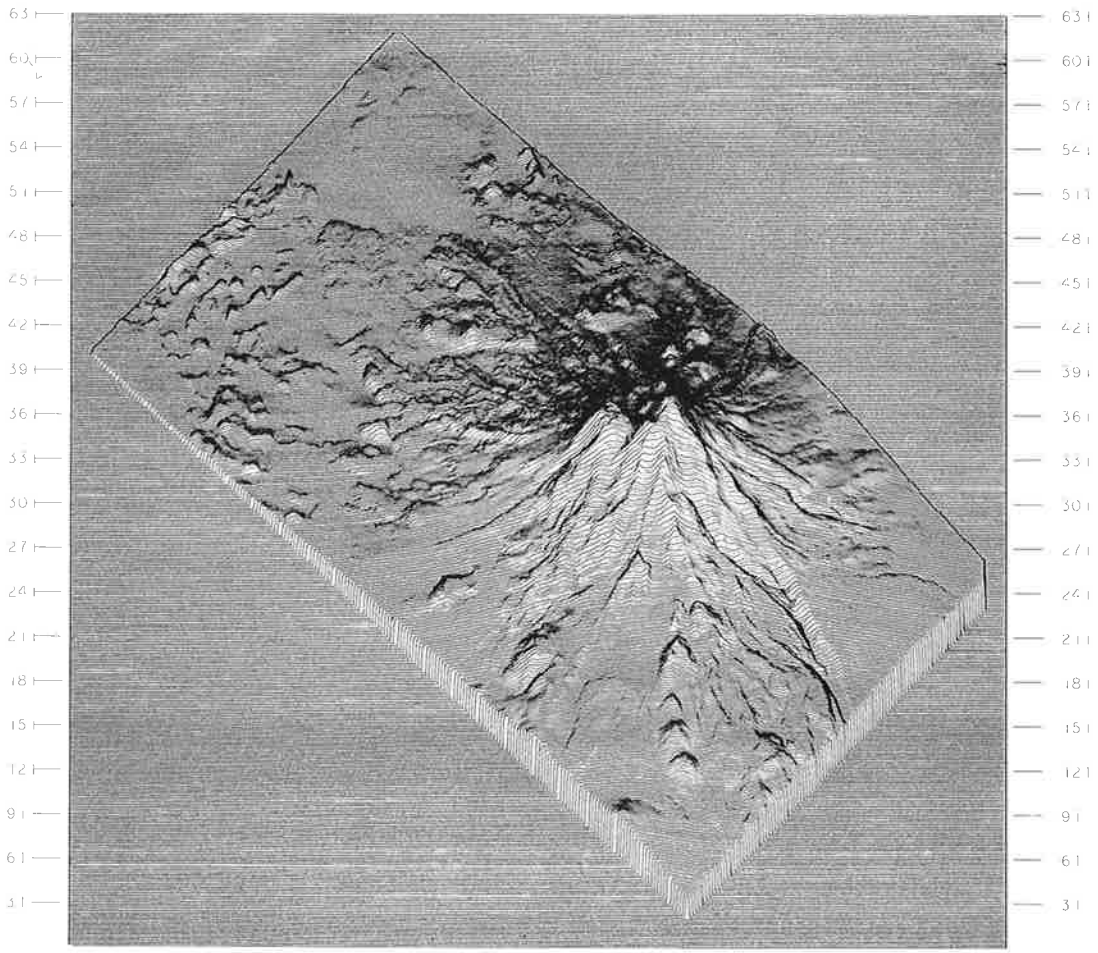

Fig. 4. Digital elevation model at a raster interval of 30 m, obtained from maps 1 : 62 500 of the area around Mt. Shasta.

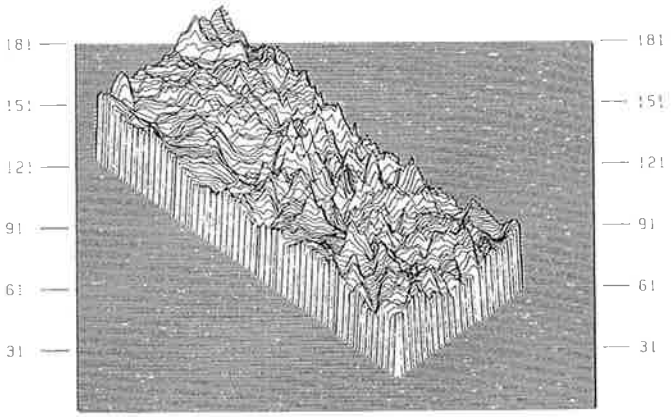


Fig. 5. Difference between the two digital elevation models of Figs. 3 and 4, at a mesh size of 150 m. The rms difference amounts to 62 m.

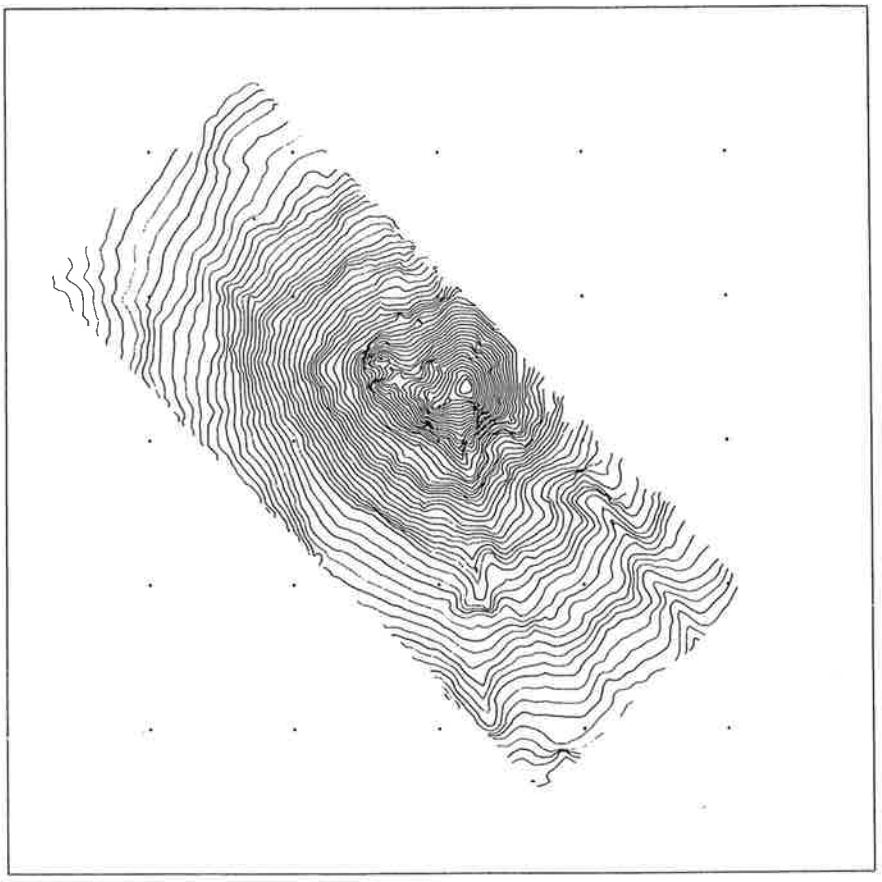


Fig. 6. Contour plot at a contour interval of 200 m, produced from the SIR-B stereo model at 51°/28° look angles.

Fig. 7. Perspective view of the radar derived DEM, with radar image brightness superimposed and coded as color.

ted as Fig. 5. A plot of computed contours at constant interval of 200 m is shown in Fig. 6. The difference DEM results in an error of 62 m. The DEM, in a perspective projection and complemented by the radar image brightness values, is presented in Fig. 7.

### *C. An Experimental Radar Image Map*

The DEM and radar image at look angle 51° off-nadir were used to create a geometrically rectified image. This is the basis for a radar image map at a scale of 1 : 100 000 containing the contour lines, limited planimetric detail and, of course, a coordinate grid and legend. Fig. 8 presents the result. The quantification of the usefulness of such mapping product will be the subject of future work.

The presentation scale of 1 : 100 000 derives from the argument that the user, with the unaided eye, will resolve less than 8 pixels/mm. Since the radar resolution is of the order of 15 m, and pixel size is 12.5 m, we find that a scale of 1 : 100 000 presents about 8 pixels on a millimeter. This, of course, is entirely unrelated to classical cartographic standards of scale and image resolution, but reflects the recent proposed scales for satellite image maps [8].

## IV. Conclusions

A scaled-down data set from the SIR-B test site around Mt. Shasta permitted the creation of a digital elevation model (DEM) and its comparison to a map-derived DEM. Root mean square height differences amount to ±60 m. This confirms the result from control points and from analysis of data from a different site in Argentina.

The paper describes the method of radar stereomodel setup and on-line data collection. It also presents an ex-

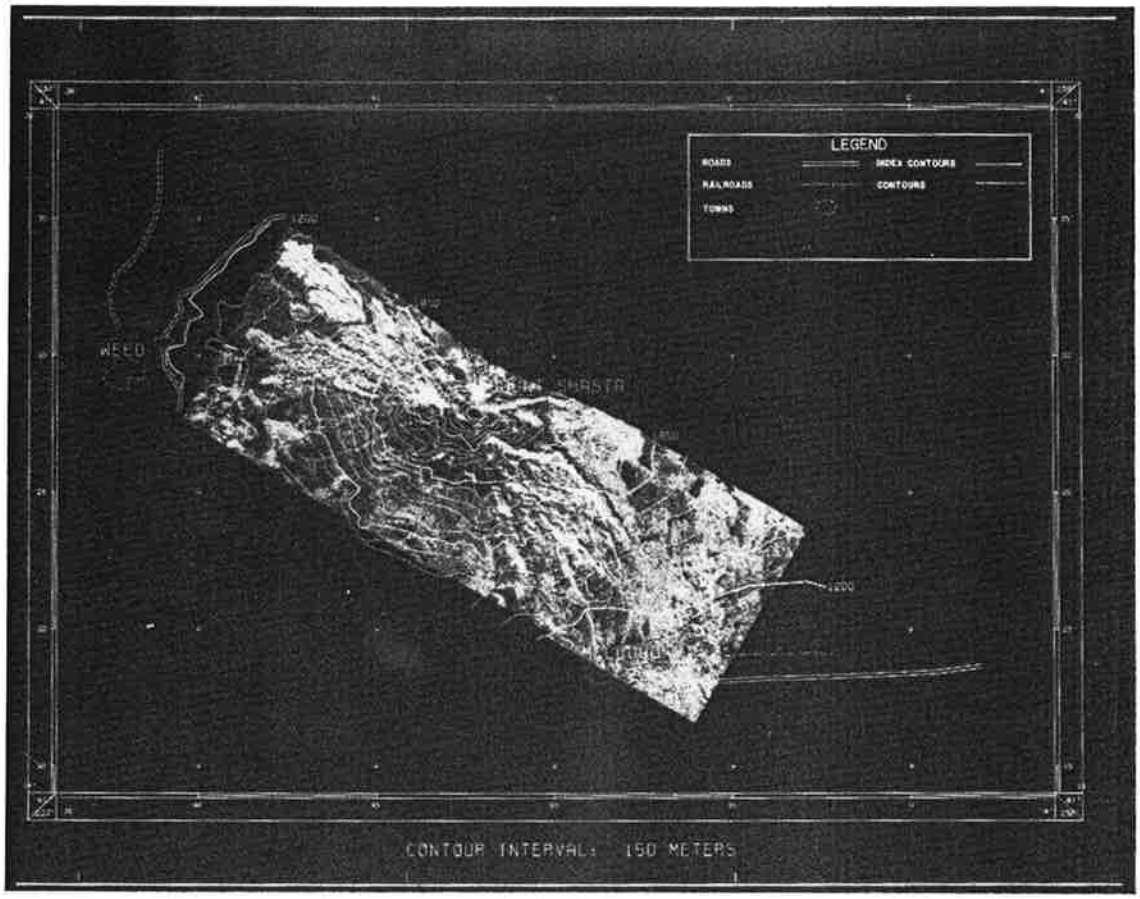


Fig. 8. Radar image map, originally at scale 1 : 100 000, with superimposed contour lines, coordinate grid, and limited planimetric detail.

perimental radar image map, originally at a scale 1 : 100 000, with contour lines at a 200-m interval.

## Acknowledgment

In the initial phases this project benefited from contributions by Dr. H. Fuchs, Graz, Austria. K. Hafner provided support in the creation of the digital elevation models.

## References

[1] K. Rinner, "Die Geometrie des Funkmessbildes," Austrian Academy of Science, 1948; *also* Handbuch der Vermessungskunde, Jordan-Eggert-Kneissl, vol. VI, Metzlersche Verlagsbuchhandlung, Stuttgart, W. Germany.

[2] D. R. Crandell, C. D. Miller, H. X. Glicken, R. L. Christiansen, and C. G. Newhall, "Catastrophic debris avalanche from ancestral Mount Shasta volcano," *Geology*, vol. 12, 1984.

[3] F. Norvelle, "AS-11-A radar program," *Photogrammetr. Eng.*, vol. 38, 1972.

[4] Autometric, "Program documentation for analytical mapping system radar model," Contract Final Rep. prepared by Autometric Inc., Falls Church, VA, for U.S. Army Engineering Topographic Laboratory, Ft. Belvoir, VA, 1982.

[5] J. Raggam and F. Leberl, "SMART—A program for radar stereo mapping of the Kern DSR-1," in *Proc. Ann. Meet. Amer. Soc. Photogrammetry*, 1984.

[6] J. Raggam, "Verfahrensentwicklung fuer Stereo-Radargrammetrie," doctoral dissertation, Technical University of Graz, A-8010 Austria, 1985.

[7] F. Leberl, G. Domik, J. Raggam, J. Cimino, and M. Kobrick, "Multiple incidence angle SIR-B experiment over Argentina: Stereo-radargrammetric analysis," *IEEE Trans. Geosci. Remote Sensing*, this issue, pp. 482–491.

[8] A. Colvocoresses, "An automated mapping satellite system (Mapsat)," *Photogrammetr. Eng. and Remote Sensing*, vol. 48, no. 10, pp. 1585–1591, Oct. 1982.

*

**Franz W. Leberl** (SM'82) was born in 1945. He received the Dipl. Ing. degree in geodetic engineering in 1967 and the Dr.Tech. degree in 1972, both from the Technical University, Vienna, Austria.

He has worked at the International Institute for Aerial Surveys and Earth Sciences, Delft and Enschede, The Netherlands, from 1969 to 1974. From 1974 to 1976, he was a Research Associate at the Jet Propulsion Laboratory, Pasadena, CA. From 1976 to 1984, he held an appointment at the Technical University, Graz, Austria, as a Professor of Photogrammetry and Remote Sensing. Simultaneously, he was Director of the Research Institute for Image Processing and Computer Graphics at the Graz Research

Center in Austria. In 1984–1985 he was with Markhurd. In 1985 he formed Vexcel Corporation in Boulder, CO. He is the author of about 100 articles.

Dr. Leberl was recipient of the Otto von Gruber Gold Medal of the International Society for Photogrammetry and Remote Sensing in 1976.

*

**Gitta Domik** was born in Graz, Austria, in 1957. She received the "Diplomingenieur" degree in 1981 and the Ph.D. degree in computer science in June 1985, both the from Technical University in Graz. Her Ph.D. dissertation dealt with analysis algorithms for digital radar imagery using elevation models.

Between 1982 and 1985, she worked in the Department of Computer Vision at the Research Center in Graz. In May 1985, she joined Vexcel Corporation in Boulder, CO, where she continues her work in radar image simulation and analysis.

*

**Johannes Raggam** received the Dipl. Ing. degree in geodetic engineering from the Technical University, Graz, Austria, in 1980 and the Ph.D. in 1985.

He is currently working on the subject of stereo radar at the Research Institute for Image Processing and Computer Graphics of the Graz Research Center, Graz, Austria. As part of his work, he developed a capability to employ a photogrammetric computer controlled stereo instrument with overlapping side-looking radar images.

*

**Michael Kobrick** received the B.S. degree in physics from Rensselaer Polytechnic Institute, the M.S. degree in astronomy from the University of Illinois, and the M.S. and Ph.D. degrees in planetary and space science from UCLA.

A research scientist at the Jet Propulsion Laboratory, his current research interests include radar remote sensing of planetary surfaces and in particular the derivation and geophysical analysis of topographic information. He is a staff scientist for the Magellan Project, a Principal Investigator on the Shuttle Imaging Radar, coinvestigator on the Mars Orbiter radar altimeter experiment, and Principal Investigator of the Digital Topographic Mapping Mission study project.

Dr. Kobrick is a member of the American Astronomical Society, Divisions for Planetary Science and Dynamical Astronomy, American Geophysical Union, AAAS, Sigma Xi American Institute of Physics, Astronomical Society of the Pacific, and the American Society of Photogrammetry, and has served on several NASA advisory panels for planetary radar as well as the Federal Interagency Coordinating Committee for Digital Cartography.